



Determining the Coordination Environment and Electronic Structure of Polymer-Encapsulated Cobalt Phthalocyanine under Electrocatalytic CO₂ Reduction Conditions using In Situ X-Ray Absorption Spectroscopy

Journal:	<i>Dalton Transactions</i>
Manuscript ID	DT-ART-04-2020-001288.R1
Article Type:	Paper
Date Submitted by the Author:	08-May-2020
Complete List of Authors:	Liu, Yingshuo; University of Michigan, Chemistry Deb, Aniruddha; University of Michigan, Department of Chemistry Leung, Kwan; University of Michigan, Department of Chemistry Nie, Weixuan; University of Michigan, Department of Chemistry Dean, William; University of Michigan, Department of Chemistry Penner-Hahn, James; University of Michigan, Department of Chemistry McCrory, Charles; University of Michigan, Department of Chemistry; University of Michigan, Macromolecular Science & Engineering Program

**Determining the Coordination Environment and Electronic Structure of Polymer-Encapsulated Cobalt
Phthalocyanine under Electrocatalytic CO₂ Reduction Conditions using *In Situ* X-Ray Absorption
Spectroscopy**

Yingshuo Liu,^{#,†} Aniruddha Deb,^{#,†,‡} Kwan Yee Leung,[†] Weixuan Nie,[†] William S. Dean,[†] James E. Penner-Hahn,^{*,†,‡}
Charles C. L. McCrory^{*,†,§}

[†] Department of Chemistry, University of Michigan, Ann Arbor, Michigan 48109, United States

[‡] Biophysics, University of Michigan, Ann Arbor, Michigan, 48109, United States

[§] Macromolecular Science & Engineering, University of Michigan, Ann Arbor, Michigan, 48109, United States

*Corresponding authors. James E. Penner-Hahn: jeph@umich.edu. Charles C. L. McCrory: cmccrory@umich.edu.

[#]These authors contributed equally to this work.

ORCID:

McCrory: ORCID: 0000-0001-9039-7192, Twitter: @McCroryLab

Penner-Hahn: ORCID: 0000-0003-0314-1274

Liu: ORCID: 0000-0003-4780-8384

Deb: ORCID: 0000-0002-0331-9709

Leung: ORCID: 0000-0002-5292-4569

Nie: ORCID: 0000-0003-2094-6840

Dean: ORCID: 0000-0002-6686-5387

Abstract

Encapsulating cobalt phthalocyanine (CoPc) within the coordinating polymer poly-4-vinylpyridine (P4VP) results in a catalyst-polymer composite (CoPc-P4VP) that selectively reduces CO₂ to CO at fast rates at low overpotential. In previous studies, we postulated that the enhanced selectivity for CO over H₂ production within CoPc-P4VP compared to the parent CoPc complex is due to a combination of primary, secondary, and outer-coordination sphere effects imbued by the encapsulating polymer. In this work, we perform *in situ* electrochemical X-ray absorption

spectroscopy measurements to study the oxidation state and coordination environment of Co as a function of applied potential for CoPc, CoPc-P4VP, and CoPc with an axially-coordinated py, CoPc(py). Using *in situ* X-ray absorption near edge structure (XANES) we provide experimental support for our previous hypothesis that Co changes from a 4-coordinate square-planar geometry in CoPc to a mostly 5-coordinate species in CoPc(py) and CoPc-P4VP. The coordination environment of CoPc-P4VP is potential-independent but pH-dependent, suggesting that the axial coordination of pyridyl groups in P4VP to CoPc is modulated by the protonation of the polymer. Finally, we show that at low potential the oxidation state of Co in the 4-coordinate CoPc is different from that in the 5-coordinate CoPc(py), suggesting that the primary coordination sphere modulates the site of reduction (metal-centered vs. ligand centered) under catalytically-relevant conditions.

Introduction

The efficient and selective electrochemical conversion of CO₂ to single products in the CO₂ reduction reaction (CO₂RR) has provoked intense scientific interest, both as a means of storing energy from intermittent energy sources such as solar and wind in the form of chemical fuels¹⁻⁶ and of recycling CO₂ in industrial waste streams into useful industrially-relevant chemical feedstocks.⁵⁻⁸ In particular, there has been significant recent research exploring the activity of cobalt phthalocyanine (CoPc) and related complexes for the CO₂RR in aqueous solutions.⁹⁻²² In general, many of these systems show high activity and selectivity for CO₂ reduction to CO,^{9-13, 16-22} and in some cases under optimized conditions and very negative potentials, the sequential reduction of CO₂ to CO to methanol.^{14, 15} However, many of these systems cast the CoPc materials onto high-surface area carbon supports such as oxidized carbon paper,^{11, 20} conductive carbon black,^{10, 12} or multi-walled carbon nanotubes,^{14, 15, 17, 23} each of which have surface functional groups that may coordinate to CoPc and influence its electronic structure and activity for the CO₂RR.^{14, 24} Moreover, many of the reported CoPc-based electrocatalyst systems use Nafion as a polymer binder,^{10-12, 14, 15, 17, 18, 20, 23} but, in general, the influence of the polymer on the coordination environment and mechanism of CoPc for the CO₂RR is not fully understood.

Our research has focused on understanding the role of encapsulating polymers on the coordination environment of CoPc, and in turn how changes in the coordination environment influence catalytic activity and reaction selectivity for the CO₂RR over competitive HER. In particular, previous investigations have shown that immobilizing cobalt phthalocyanine (CoPc), an active but non-selective catalyst for the CO₂RR in aqueous

phosphate electrolyte,^{9, 25, 26} within a poly-4-vinylpyridine (P4VP) polymer on a graphite electrode dramatically increases the complex's catalytic activity and selectivity for the CO₂RR.^{9, 26, 27} We have shown that the resulting CoPc-P4VP system is a highly active and selective electrocatalytic system for the reduction of CO₂ to CO.⁹ The increased activity and selectivity of CoPc-P4VP has been attributed to three effects of P4VP on the coordination environment of the CoPc complex as shown in Figure 1.^{9, 27} First, in the catalyst's primary coordination sphere, axial coordination of pyridyl groups in P4VP to the Co-center of CoPc increases the catalyst's nucleophilicity and promotes CO₂ binding. Second, in the catalyst's secondary coordination sphere, protonated pyridyl groups in P4VP stabilize coordinated CO₂RR intermediates via H-bonding interactions. Third, in the catalyst's outer coordination sphere, H⁺ transport to the catalyst active site occurs via a proton relay mechanism involving pyridyl groups in P4VP.

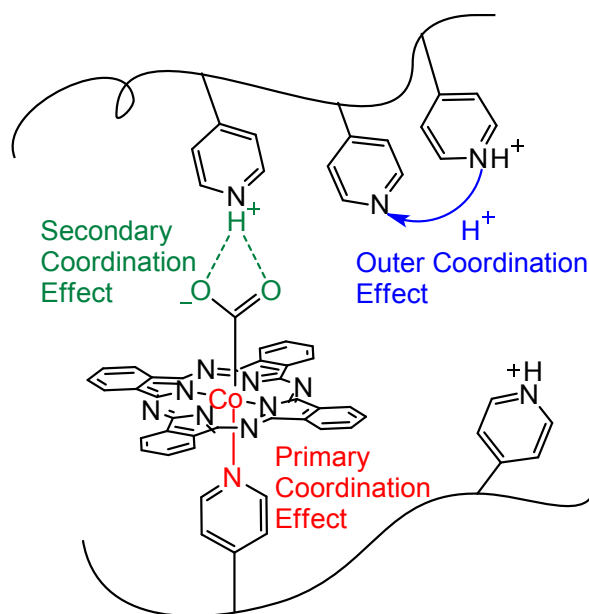
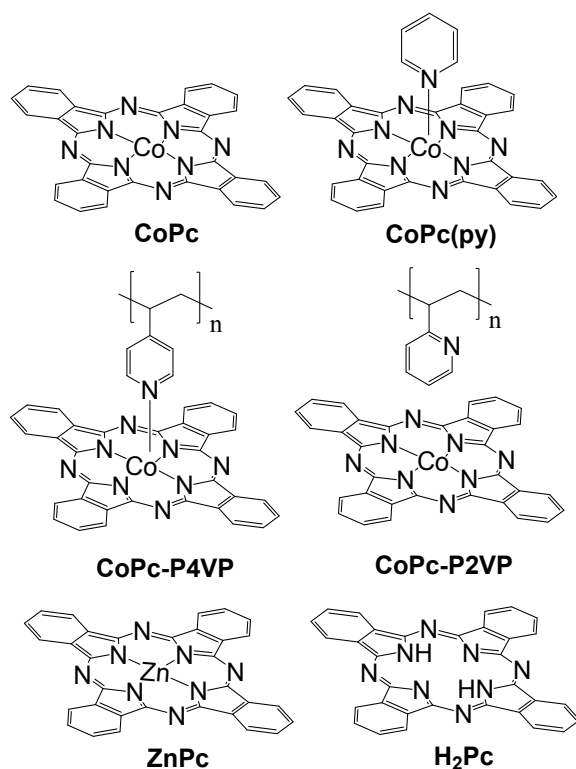


Figure 1. An illustration of CoPc encapsulated in P4VP highlighting the primary, secondary, and outer coordination sphere effects.

The effect of the coordination environment on the enhanced activity and selectivity of CoPc-P4VP for the CO₂RR has been supported by recent electrochemical mechanistic and kinetic studies.^{9, 19} In particular, the axial ligation of the pyridyl groups in the P4VP polymer to CoPc play a crucial role in the catalytic mechanism for the CO₂RR. CoPc-P4VP reduces CO₂ with 3-4 times the activity of the parent CoPc complex^{25,26} due to a shift in the

rate determining step of the catalytic mechanism from an initial CO₂ binding step to a subsequent protonation event upon axial coordination of the pyridyl groups to CoPc.²⁶ In contrast, in CoPc-P2VP, CoPc is immobilized in a P2VP polymer such that axial coordination of the polymer pyridyl groups to CoPc is sterically hindered (see Scheme 1). The CoPc-P2VP system reduces CO₂ with no enhancement of activity relative to the parent CoPc complex due to the lack of axial coordination from the P2VP pyridyl groups to the CoPc.^{25,26} An implicit assumption in our previous studies is that CoPc-P4VP exists primarily as a 5-coordinate complex under our catalytic conditions, whereas CoPc-P2VP exists primarily as a 4-coordinate complex under identical conditions. Moreover, we assumed that the coordination environment of the CoPc does not change under electrocatalytic CO₂ reduction conditions. The work presented here provides direct evidence supporting for these previous assumptions.



Scheme 1. Catalyst and polymer-catalyst composite systems investigated in this work along with their postulated axial coordination.

In this study, we measure the coordination environment of CoPc-P4VP both as deposited and under electrocatalytic CO₂ reduction conditions using *in situ* X-ray absorption spectroscopy (XAS). In particular, we use

X-ray absorption near edge structure (XANES) measurements to characterize the coordination geometry and oxidation state of the Co center in CoPc-P4VP and related systems (Scheme 1) adsorbed onto carbon supports and under applied electrochemical potential both in the presence and absence of CO₂. We show that the parent CoPc complex and the composite CoPc-P2VP film show an intense pre-edge feature in the Co K-edge XANES spectra associated with a 1s-4p pre-edge peak characteristic of square-planar macrocyclic Co complexes as expected for these systems. However, for CoPc(py) and CoPc-P4VP, where we expect a 5-coordinate square pyramidal structure, we observe a dramatic decrease in the 1s-4p pre-edge peak intensity consistent with conversion from square-planar geometry to a 5-coordinate square-pyramidal complex. The steady-state coordination geometry of the CoPc-P4VP remains constant regardless of applied potential and even in the presence of CO₂ under electrocatalytic conditions.

In addition, we have measured the oxidation state of the Co in CoPc, CoPc-P4VP and related systems as a function of applied potential. Specifically, we show that the first oxidation and first reduction of the adsorbed 5-coordinate CoPc(py) species have metal-based character, which are consistent with the findings of previous theoretical studies^{10, 28} and previously proposed catalytic mechanisms for the CO₂RR by CoPc that assert an initial Co-based reduction.^{11, 26, 27, 29-32} However, in the case of 4-coordinate CoPc, we find that the energy of the Co K-edge does not change as a function of applied potential, suggesting that redox events in CoPc are ligand-based under our conditions. This is an interesting result that differs from the findings of previous reports for CoPc,^{10, 11, 26-32} but is not entirely unknown for cobalt complexes with redox-active ligands.³³⁻³⁵ We discuss the implications of the XAS results on the catalytic mechanism for the CO₂RR by CoPc and conduct additional experiments to assess the importance of the Co center on the CO₂RR in the CoPc system.

Experimental

Materials and Chemicals

All purchased chemicals were used as received unless otherwise specified. Cobalt phthalocyanine (CoPc, 97%), poly-4-vinylpyridine (P4VP, average Mw ~ 160,000), poly-2-vinylpyridine (P2VP, average Mw ~ 159,000), N,N-dimethylformamide (DMF, ACS grade), pyridine (ACS grade, ≥ 99%), dimethyl sulfoxide (DMSO, ACS grade, ≥ 99.9%), Zinc phthalocyanine (ZnPc, 97%), H₂-phthalocyanine (H₂Pc, 98%), ferrocenecarboxylic acid (97%),

sodium phosphate monobasic (NaH_2PO_4 , BioXtra, > 99%), sodium hydroxide (NaOH , BioXtra, $\geq 98\%$), phosphoric acid (H_3PO_4 , ≥ 85 wt. % in H_2O , $\geq 99.999\%$ trace metals basis), boron nitride, and Nafion-117 cation exchange membrane (Nafion) were purchased from Sigma Aldrich. Tetrabutylammonium hexafluorophosphate (nBu_4NPF_6 , > 98.0%) was purchased from TCI America and recrystallized from Methanol/ H_2O (v/v = 8/1). Edge plane graphite disk electrodes (EPG, 5 mm diameter, effective electrode surface area: 0.114 cm^2) were purchased from Pine Research Instrumentation. Carbon paper (AvCarb P50) was purchased from the Fuel Cell Store. Carbon rods were purchased from Strem Chemicals, Inc. Pt wire (99.99%, 0.02" diameter) was purchased from Surepure Chemetals L.L.C. Compressed CO_2 gas (99.8%) was purchased from Cryogenic Gases. All water used in this study was ultrapure water ($18.2 \text{ M}\Omega\text{-cm}$ resistivity) purified with a Thermo Scientific GenPure UV-TOC/UF xCAD-plus water purification system.

Preparation of CoPc and CoPc(py) Standard Complexes

The 4-coordinate CoPc complex was purified using a previously reported preparation by heating the as-purchased complex at $\sim 210 \text{ }^\circ\text{C}$ under vacuum for 24 h.³⁶ The 5-coordinate CoPc(py) complex was synthesized using a previously reported preparation by first heating CoPc in pure pyridine under reflux until the CoPc solid was fully dissolved, then cooling the system to $100 \text{ }^\circ\text{C}$ to obtain a precipitate that was filtered and dried under vacuum.³⁷ Both the 4-coordinate CoPc and 5-coordinate CoPc(py) standard complexes were characterized by elemental analysis conducted by Midwest Microlab, Inc. Anal. Calcd (found) for CoPc, ($\text{C}_{32}\text{H}_{16}\text{CoN}_8$): %C 67.25 (66.97), %H 2.82 (2.96), %N 19.61 (19.45). Anal. Calcd (found) for CoPc(py), ($\text{C}_{37}\text{H}_{21}\text{CoN}_9$): %C 68.30 (67.98), % H 3.25 (3.26), % N 19.38 (19.21).

Preparation of Modified Carbon Paper Electrodes

CoPc: The CoPc/DMF deposition solution was prepared by dissolving 3 mg of CoPc in 100 mL DMF. The resulting solution was sonicated for 30 min to fully disperse the CoPc. CoPc coated carbon paper electrodes were prepared by drop-casting a total volume of 2.5 mL of the CoPc/DMF deposition solution to form a 3 cm diameter circular coating on a carbon paper disk of 6.5 cm diameter. The DMF solvent was evaporated by flowing N_2 gas over the sample at room temperature for ~ 4.5 h. The resulting Co loading was $\sim 1.9 \times 10^{-8} \text{ mol cm}^{-2}$. The CoPc coated carbon paper electrodes are designated CoPc/CP.

CoPc(py): The CoPc(py) deposition solution was prepared by dissolving 3 mg of CoPc in 5 mL of pyridine. The resulting solution was sonicated for 30 min to fully disperse the CoPc. CoPc(py) coated carbon paper electrodes were prepared by drop-casting a total volume of 0.125 mL of the CoPc(py) deposition solution to form a 3 cm diameter circular coating on a carbon paper disk of 4 cm diameter. The extra pyridine solvent was evaporated by flowing N₂ gas over the sample at room temperature for ~4.5 h. The resulting Co loading was $\sim 1.9 \times 10^{-8}$ mol cm⁻². The CoPc(py) coated carbon paper electrodes are designated CoPc(py)/CP.

CoPc-P4VP (P2VP): The CoPc-P4VP (1% w/v) and CoPc-P2VP (1% w/v) deposition solutions were prepared by dissolving 0.025 g of P4VP (or P2VP) in 2.5 mL of the CoPc/DMF solution. The resulting solution was sonicated for 20 mins to fully dissolve the P4VP (or P2VP) and disperse the CoPc. CoPc-P4VP (or CoPc-P2VP) coated carbon paper electrodes were prepared by drop-casting a total volume of 2.5 mL of the CoPc-P4VP/DMF (or CoPc-P2VP/DMF) deposition solution to form a 3 cm diameter circular coating on a carbon paper disk of 4 cm diameter. The DMF solvent was evaporated over N₂ gas at room temperature for ~4.5 h. The resulting Co loading was $\sim 1.9 \times 10^{-8}$ mol cm⁻². The CoPc-P4VP and CoPc-P2VP coated carbon paper electrodes are designated CoPc-P4VP/CP and CoPc-P2VP/CP, respectively.

Electrolyte Solution Preparation

All electrolyte solutions were prepared using ultrapure water. The pH 3 phosphate solutions were prepared from a 0.1 M NaH₂PO₄ solution adjusted to pH 3 by the addition of 1 M H₃PO₄ solution. The pH 5, 7, and 9 phosphate solutions were prepared from a 0.1 M NaH₂PO₄ solution adjusted to the appropriate pH by the addition of 1 M NaOH solution. All solution pH were measured using a Thermo Scientific™ Orion™ 2 STAR pH meter with a Triode™ pH/ATC electrode (9157BNMD) calibrated with a three-point calibration curve at pH = 4.01, 7.00, and 10.01.

X-ray Absorption Spectroscopy

X-ray absorption spectra were measured at SSRL beamline 7-3, with a Rh coated Si harmonic rejection mirror set to E_c = 12 keV, and a fully-tuned Si[220] double-crystal monochromator... The incident intensity was monitored using a N₂ filled ion chamber, and the energy was calibrated by simultaneous measurement of the absorption spectrum of a Co foil inserted downstream of the sample. X-ray absorption for the electrochemical samples was measured as fluorescence excitation spectra using a solid-state energy-resolving 30-element Ge detector. In

addition, transmission mode measurements were made on solid samples of CoPc and CoPc(py), prepared by grinding to a fine powder in BN. X-ray absorbance for all samples was measured by scanning in steps of: 10 eV over the pre-edge (7479-7689 eV), 0.25 eV over the edge (7689-7739 eV) and steps of 1.0 above the edge. The relatively low concentration of Co on the electrodes precluded measurement of EXAFS spectra.

All of the fluorescence channels of each spectrum were analyzed to ensure the absence of artifacts and then averaged. The XANES spectra were then normalized using the tabulated Co-K absorption cross-sections below (7490-7690 eV) and well above (7790-8200 eV) the edge-region³⁸ using a single cubic polynomial which is interpolated through the XANES region and scaled using a single scale factor with the M-BACK program.³⁹

***In Situ* Electrochemical XAS Measurements**

The *in situ* electrochemical XAS measurements were performed using a custom-made XAS cell (Figure S1) using a Bio-Logic SP200 potentiostat, and the electrochemical data was recorded using the Bio-Logic EC-Lab v10.44 software package. The XAS cell chamber held ~40 ml of solution, and the X-ray path length in the cell was ~1 mm to minimize the attenuation of the incident beam. Measurements were performed using an aqueous electrolyte of pH 5 phosphate solution unless otherwise indicated. CoPc, CoPc(py), CoPc-P2VP, and CoPc-P4VP were drop-cast onto carbon paper as described above. Note that CoPc is essentially insoluble in water^{40, 41} so no aqueous solution phase measurements were attempted—the CoPc and related systems were always deposited onto a high-surface area carbon support for the aqueous measurements.

The *in situ* electrochemical XAS measurements consisted of a series of controlled-potential electrolysis experiments between 1.2 V and -1.25 V vs SCE. Unless otherwise noted, the working electrode was the catalyst-modified carbon paper, the reference electrode was a commercial saturated calomel electrode (SCE, CH-Instruments) externally referenced to ferrocenecarboxylic acid in 0.2 M phosphate buffer at pH 7 (0.284 V vs. SCE),⁴² and the auxiliary electrode was a carbon rod (99.999%, Strem Chemicals Inc.). Prior to each controlled potential electrolysis (CPE) experiment, the cell was flushed with CO₂ or N₂ for ~40 min and then the headspace was blanketed with a flow of CO₂ or N₂ during the measurements. The CO₂ or N₂ used was saturated with electrolyte solution by bubbling through a gas washing bottle filled with the same electrolyte solution used in the XAS cell to minimize electrolyte evaporation in the cell during the course of the measurements. When saturated with CO₂, the pH 5 electrolyte solution had a measured pH = 4.7. The uncompensated resistance of the cell was measured with

a single-point high-frequency impedance measurement, and all electrochemical CPE measurements were automatically iR -compensated at 85% through positive feedback using the Bio-Logic EC-Lab software. In general, our XAS electrochemical cell had an uncompensated resistance $R_u = \sim 10 \Omega$ in pH 5 phosphate electrolyte solution. The solutions were not stirred during the CPE experiments. After each potential change, the system was held at the new potential for ~ 15 - 20 min to allow the system to reach steady-state before XAS data was collected.

Cyclic Voltammetry (CV) of Modified EPG Electrodes

Cyclic Voltammetry (CV) experiments of modified EPG electrodes were conducted in a glass two-chamber cell under N_2 or CO_2 . The working electrodes were catalyst-modified EPG electrodes, the reference electrode was a commercial SCE, and the auxiliary electrode was a carbon rod separated from the working and reference electrodes by a Nafion membrane. The scan rate was 0.2 V/s, and the CVs were iR compensated at 85% through positive feedback using the EC-Lab software.

Prior to modification, 5 mm diameter EPG disk electrodes were manually polished on 600 grit SiC grinding paper (Buehler, Carbimet Plain) followed by sonication in ultrapure water for ~ 1 min. The same CoPc, CoPc-P4VP, and CoPc(py) deposition solutions used for the preparation of the catalyst-modified carbon paper electrodes were used for the preparation of the catalyst-modified EPG electrodes. Catalyst-modified EPG electrodes were prepared by drop-casting $5 \mu L$ of the appropriate deposition solutions onto the EPG electrodes. The disk electrodes were then placed in an oven at ~ 70 °C for ~ 15 minutes to allow the solvent to evaporate.

Sealed-Cell Controlled Potential Electrolyses of Modified EPG Electrodes with ZnPc and H₂Pc

Prior to modification, 5 mm diameter EPG disk electrodes were manually polished on 600 grit SiC grinding paper (Buehler CarbiMet) followed by sonication in ultrapure water for ~ 1 min. Modified working electrodes were prepared by first drop-casting $5 \mu L$ 0.05 mM ZnPc or 0.05 mM H₂Pc deposition solution onto EPG electrode. The disks electrodes were then placed in an oven at ~ 70 °C for ~ 15 minutes to allow the solvent to evaporate.

The deposition solutions for P4VP-encapsulated ZnPc or H₂Pc were prepared by dissolving 0.025 g of P4VP in 2.5 mL of either 0.05 mM ZnPc/DMF or 0.05 mM H₂Pc/DMF solution. Modified working electrodes for polymer encapsulated catalysts were prepared by drop-casting $5 \mu L$ ZnPc-P4VP/DMF or H₂Pc-P4VP/DMF deposition solution onto EPG electrode, followed by heating in the oven at ~ 70 °C for ~ 15 minutes to allow the solvent to

evaporate. Controlled potential electrolyses (CPE) were conducted at room temperature in a custom, gas-tight, two-chamber U-cell as previously described.¹⁹ The main chamber held the modified working electrode and an SCE reference electrode. The auxiliary chamber held the auxiliary carbon rod electrode. The two chambers were separated with a Nafion cation exchange membrane. Prior to each experiment, the electrolyte in both chambers was sparged with CO₂ for ~30 min before the main chamber was sealed under CO₂ atmosphere. The CPE experiments were conducted with no *iR* compensation for solution resistance, and the reported electrolysis potentials are the actual applied potentials. The uncompensated resistance of the cell was measured with a single-point high-frequency impedance measurement. In general, our electrochemical cell for CPE had an uncompensated resistance $R_u = \sim 200 \Omega$ in pH 5 phosphate electrolyte solution. The product detection and quantification were conducted as previously described.¹⁹ All experiments were performed at least three times with independently prepared electrodes, all reported values are the averages of these repetitions, and uncertainties are reported as standard deviations.

Results and Discussion

Our lab^{9, 19} and others^{26, 27} have shown that encapsulating CoPc within a coordinating polymer such as P4VP results in a dramatic increase in activity and selectivity for the CO₂RR over competitive hydrogen evolution. This difference in CO₂RR activity and selectivity for the CoPc-P4VP catalyst-polymer composite compared to the parent CoPc complex has been attributed to changes in the coordination environment surrounding the CoPc complex in the polymer.^{9, 19, 26, 27, 43} In particular, we have previously proposed that axial coordination of pyridyl groups from the P4VP to the Co center in CoPc is partially responsible for the increased activity and selectivity of CoPc-P4VP compared to CoPc.^{9, 19} In this work, we use *in situ* electrochemical XAS measurements to experimentally verify the coordination environment of Co in CoPc-P4VP and related systems under electrocatalytically-relevant conditions and potentials.

Normalized XANES measurements were compared under different conditions over the range of 7705–7755 eV. Information about the electronic structure and Co-coordination environment of each sample was determined by comparing to standard compounds of CoPc and CoPc(py). For each set of measurements, the electrochemical XAS cell was assembled with freshly prepared electrodes. Note that it has been previously reported that CoPc

undergoes significant aggregation when adsorbed onto carbon surfaces at high loadings which influences the observed activity per Co site¹¹, but does not influence the catalytic mechanism.¹⁹ In our system, CoPc,¹⁹ CoPc-P4VP,¹⁹ and CoPc(py) (Figure S2) all show similar extents of aggregation at our Co loadings, suggesting that any observed differences in the measured XANES spectra for these three systems cannot be explained by differences in extent of aggregation.

The XANES spectra can be characterized by two peaks, a weaker 1s-3d pre-edge peak at ~7710 eV and a stronger 1s-4p pre-edge peak at ~7716 eV. The former is found to increase in intensity as a metal site distorts from centrosymmetric to non-centrosymmetric coordination environment; this is interpreted as resulting from an increase in 3d+4p mixing in the non-centrosymmetric environment. The intensity and position of the 1s-3d peak has been used to confirm the oxidation state of Co complexes in other studies,^{44, 45} but the low concentration of catalyst sites adsorbed to the carbon paper electrodes in our system leads to 1s-3d peaks that lack sufficient intensity to perform such an analysis. The 1s-4p peak is characteristic of square-planar complexes⁴⁶ and has been interpreted as either 1s-4p+shakedown^{47, 48} or a direct 1s-4p transition.⁴⁹ Regardless of the assignment, it is well-established that this peak is characteristic of macrocyclic Co complexes with Co in square-planar environments,^{10, 48} with significantly decreasing intensity when complexes go from square-planar to square-pyramidal and finally to octahedral geometries (this peak is also weak for tetrahedral complexes,⁴⁶ but those are not considered further here, given the rigidity of the phthalocyanine ring). The XANES spectra of CoPc and CoPc(py) standards are shown in Figure 2. The XANES of the CoPc standard shows the typical 4-coordinate strong pre-edge (1s-4p) peak at ~7716 eV, while coordination in the CoPc(py) standard shows a weak pre-edge peak at ~7716 eV, which is consistent with a conversion from a square-planar Co geometry to a 5-coordinate square-pyramidal CoPc(py) complex.^{11, 19}

Coordination Environment of Polymer-Encapsulated CoPc Complexes

In previous studies, CoPc was investigated as a CO₂RR catalyst in aqueous solution when either directly adsorbed onto an electrode surface, adsorbed as CoPc(py) with an axially-coordinated pyridine, or immobilized onto the surface after encapsulating it in a coordinating P4VP or non-coordinating P2VP polymer. We previously hypothesized that the Co center in CoPc and CoPc-P2VP had a 4-coordinate geometry, and the CoPc(py) and CoPc-P4VP existed in a 5-coordinate geometry with an axially-coordinated pyridyl residue.^{9, 19, 26, 27} In this study, we experimentally determined the coordination environment of the parent CoPc, CoPc(py), CoPc-P4VP, and CoPc-

P2VP all adsorbed onto a carbon paper (CP) support and exposed to pH 5 phosphate solutions. The coordination environment was characterized using the relative intensity of the 1s-4p peak. The XANES spectra for these samples, along with those for the CoPc and CoPc(py) standards are shown in Figure 2. CoPc/CP shows a strong 1s-4p peak at 7716 eV consistent with a 4-coordination Co center, whereas CoPc(py)/CP and CoPc-P4VP/CP have nearly identical spectra with a weak peak indicating primarily 5-coordinate Co in these systems. The spectrum for CoPc-P2VP/CP is nearly identical to that for CoPc/CP, suggesting that the Co remains 4-coordinate in the non-coordinating P2VP polymer. These XANES results experimentally verify our previous hypothesis that Co exists as a 4-coordinate species in CoPc and CoPc-P2VP, and a 5-coordinate species in CoPc-P4VP and when CoPc(py) is deposited directly onto graphite surfaces.^{9, 19} The small differences between the spectra for the surface adsorbed samples and the reference CoPc and CoPc(py) dry standards may indicate either an equilibrium between 4- and 5-coordinate species in the coated samples or alternatively may simply reflect the sensitivity of XANES to longer distance interactions which vary between the microcrystalline reference standard compounds and the coated samples. Note that CoPc has been reported to axially-coordinate to activated carbon supports such as carbon nanotubes as evidenced by a decrease in the intensity of the 1s-4p_z peak in the Co K-edge spectra.¹⁴ Our data demonstrates that the majority of the Co is 4-coordinate in CoPc/CP and not axially-coordinated to the carbon surface. However, we cannot exclude the possibility that a small fraction of the CoPc coordinates to an oxide species on the carbon paper forming an active species for CO₂RR.

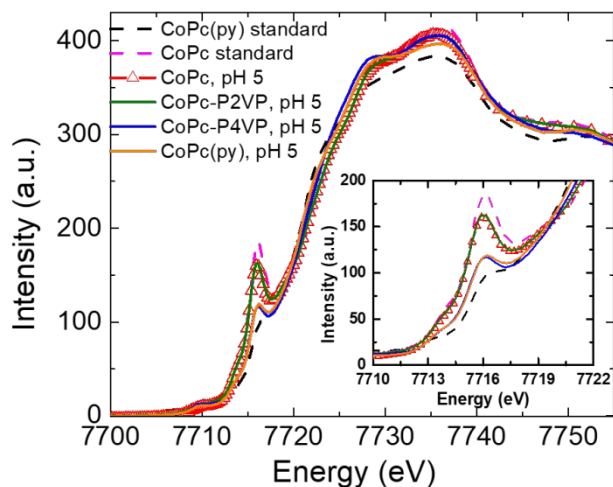


Figure 2. XANES spectra of CoPc/CP, CoPc-P2VP/CP, CoPc-P4VP/CP, and CoPc(py)/CP immersed in pH 5 phosphate electrolyte solution. XANES measurements of independently synthesized 4-coordinate CoPc and pure 5-coordinate CoPc(py) dry powders are included as standards. The inset is a zoom-in of the 1s-4p peak at 7716 eV. An strong peak at 7716 eV is characteristic of Co in a square planar geometry as observed for CoPc/CP and CoPc-P2VP/CP, whereas a weak peak is associated with Co in a non-square planar geometry as observed for CoPc(py)/CP and CoPc-P4VP/CP. In the case of CoPc(py)/CP and CoPc-P4VP/CP, we attribute this non-square planar geometry to formation of a 5-coordinate Co species upon axial ligation to pyridine or polymer-pyridyl groups, respectively.

Coordination Environment of CoPc/CP and Related Systems as a Function of pH

As solution pH changes, there will be corresponding change in fractional protonation of pyridyl groups in P4VP.²⁷ This, in turn, may modulate the extent of coordination of pyridyl groups to CoPc in CoPc-P4VP—in more acidic solutions, fewer unprotonated pyridyl groups may be available to coordinate Co in CoPc-P4VP. To investigate how the coordination environment of CoPc in P4VP and in CoPc(py) is modulated by pH, Co K-edge XANES were measured for CoPc(py)/CP and CoPc-P4VP/CP as a function of pH at open circuit potential under N₂. In the CoPc(py)/CP sample exposed to phosphate solution (Figure 3a), there is a stronger 1s-4p peak at every pH compared to the dry CoPc(py) standard. This increased intensity of the 1s-4p peak for CoPc(py)/CP exposed to phosphate solution suggests that any exposure to electrolyte results in loss of some fraction of the coordinated pyridines. When CoPc(py)/CP is exposed to pH 3, the intensity of the 1s-4p peak is greatest, and thus loss of coordination to the pyridine is largest. We postulate that at pH 3, the protonation of pyridine ($pK_a = 5.2$)⁵⁰ is favored which facilitates dissociation of pyridine from CoPc(py). At pH ≥ 5 , we expect the pyridine groups in CoPc(py) should remain largely deprotonated and thus we expect a larger fraction of the CoPc(py) will remain 5-coordinate. This postulate is supported by the XANES measurements which show a decreased intensity of the 1s-4p peak for CoPc(py) exposed pH ≥ 5 solutions consistent with increased 5-coordinate character compared to that of CoPc(py) exposed to pH 3 solution.

In contrast, the CoPc-P4VP/CP sample does not exhibit the same extent of pH-dependent change in coordination environment as does CoPc(py). In particular, the CoPc encapsulated in P4VP shows only a slight decrease in 5-coordinate species with decreasing pH (Figure 3b), which we attribute to the influence of the polymer conformation on the effective pK_a of the Co-bound pyridyl groups. In order to confirm that the axial ligation in CoPc-P4VP comes from the backbone pyridyl groups, a control experiment was conducted with CoPc encapsulated in P2VP. The Co XANES of CoPc-P2VP/CP under different pH conditions are shown in Figure 3c. Here the shape and the position of the pre-edge is preserved, indicating that CoPc remains 4-coordinate throughout the pH range of 9 to 3, which is consistent with the conclusion that P2VP does not coordinate with CoPc because of the steric hindrance.

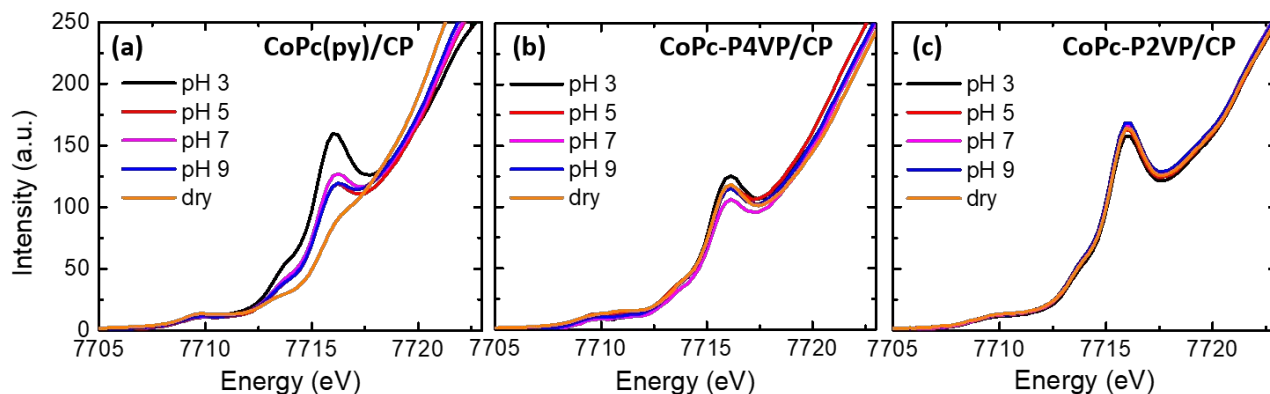


Figure 3. Pre-edge spectra near 7716 eV of (a) CoPc(py)/CP, (b) CoPc-P4VP/CP, and (c) CoPc-P2VP/CP exposed to phosphate solutions at different pH under N_2 atmosphere at open circuit potential.

Coordination Environment and Oxidation State of CoPc/CP and Related Systems as a Function of Applied Potential

To determine whether the CoPc remains 5-coordinate in P4VP polymer and in CoPc(py) during the course of reduction as we previously proposed,⁹ we measured XANES for CoPc/CP, CoPc(py)/CP, and CoPc-P4VP/CP exposed to pH 5 phosphate electrolyte solution as a function of applied potential. The electrochemical redox potentials of CoPc immobilized on an edge plane graphite electrode (CoPc/EPG) in pH 5 phosphate electrolyte solution were evaluated using Cyclic Voltammetry (CV) as shown in Figure 4. The observed CV is consistent with those previously reported for this system.⁹ The broad quasi-reversible peaks at 0.50 V and -0.34 V vs. SCE are assigned to the oxidation and first reduction of CoPc, respectively. The second reduction at ~ -1.1 V is the onset potential for HER and/or CO_2 RR under both N_2 and CO_2 . Note that CoPc-P4VP and CoPc(py) immobilized on EPG exposed to pH 5 phosphate electrolyte show similar CV features as CoPc, as shown in Figure S3-S4. Sequential *in situ* Co K-edge XANES measurements were made while holding the CoPc/CP and related modified electrodes at 1.2 V (oxidized complex), 0 V (neutral complex), -0.5 V (singly-reduced complex), and -1.25 V (doubly-reduced complex) vs. SCE as shown in Figure 5. The corresponding chronoamperometry data are shown in Figure S5-S10.

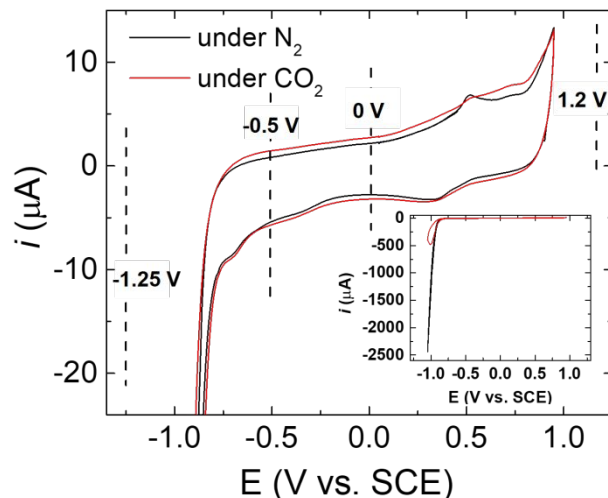


Figure 4. Cyclic voltammogram (CV) of CoPc/EPG electrode in pH 5 phosphate electrolyte under both N_2 and CO_2 atmospheres. The main figure shows the main electrochemical features preceding catalysis, and the inset shows the catalytic features as well.

The XANES spectra for the CoPc/CP system (Figure 5a-b) show a strong 1s-4p peak at 7716 eV suggesting the steady-state coordination environment surrounding Co remains primarily 4-coordinate at all applied potentials under both N_2 and CO_2 . In comparison, the CoPc(py)/CP system (Figure 5c-d) and the CoPc-P4VP/CP system (Figure 5e-f) both show a much weaker 1s-4p peak suggesting that the steady-state coordination environment surrounding Co remains primarily 5-coordinate in these systems at all potentials in both N_2 and CO_2 . These studies show that the steady-state coordination environment is largely potential-independent and is dictated by the coordination of pyridine or the pyridyl groups in P4VP, rather than transiently-associating ligands like CO_2 under electrocatalytic conditions.

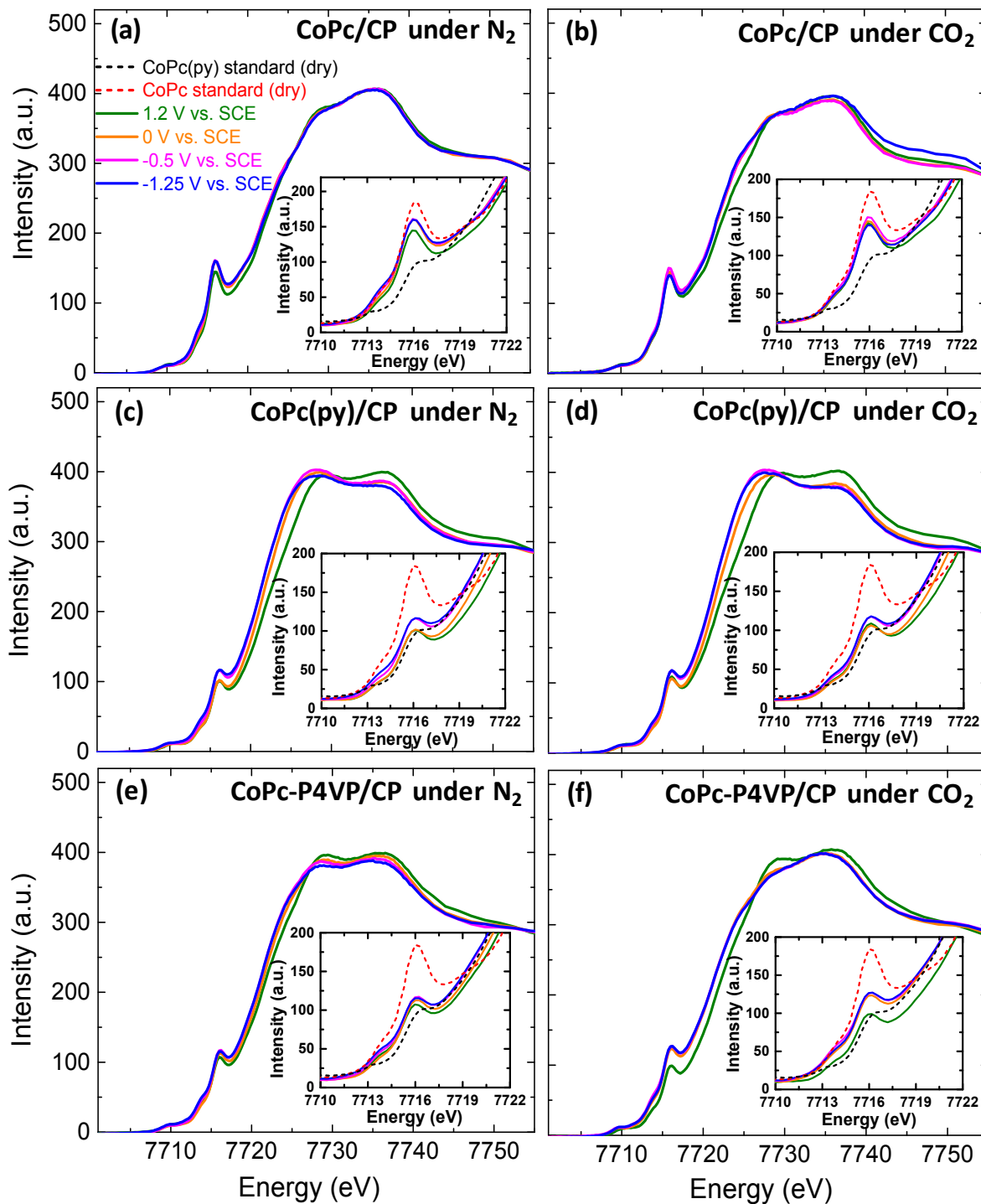
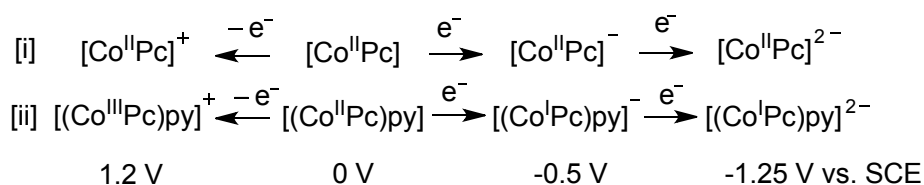


Figure 5. *In situ* XANES spectra of CoPc-based systems absorbed onto carbon paper electrodes and exposed to pH 5 phosphate electrolyte solution at four different potentials: (a) CoPc/CP under N₂, (b) CoPc/CP under CO₂, (c) CoPc(py)/CP under N₂, (d) CoPc(py)/CP under CO₂, (e) CoPc-P4VP/CP under N₂, (f) CoPc-P4VP/CP under CO₂. The inset in each panel is the zoomed-in region showing the 1s-4p features near 7716 eV.

In addition, in the case of CoPc/CP, the energy and shape of the Co K-edge does not appreciably change as a function of applied potential under either N₂ or CO₂ (Figure 5a-b), suggesting the oxidation and reduction events at CoPc are primarily ligand based under these conditions and do not involve a formal change in the oxidation state of the Co center as illustrated in Scheme 2 [i], except a small increase in oxidation state upon oxidation under CO₂. For comparison, in the case of CoPc(py)/CP, the energy of the XANES edge shifts as a function of applied potential under N₂ and CO₂ (Figure 5c-d). In particular, starting at the neutral complex at 0 V vs SCE, as we apply a more positive potential of 1.2 V vs SCE there is an edge shift to higher energy, indicative of an increase in the average Co oxidation state. Likewise, when we apply a more negative potential of -0.5 V vs SCE, we observe an edge shift to lower energy indicative of a decrease in the average Co oxidation state. However, there is no additional change in edge position when applying an even more negative potential of -1.25 V vs SCE. These results suggest that the oxidation and first reduction of the CoPc(py)/CP system involve changes in the Co oxidation state, but the second reduction is largely ligand-based as illustrated in Scheme 2 [ii].



Scheme 2. Proposed electrochemical mechanism for 4-coordinate [i] and 5-coordinate [ii] CoPc at different applied potentials with individual oxidation states on the Co center.

Previously proposed mechanisms for CoPc-catalyzed CO₂ reduction suggest that the first two electrochemical processes are Co-based (Co^{III/II} and Co^{II/I}), whereas the third is ligand-based, analogous to the process shown in Scheme 2 [ii].^{26, 29-31} This is qualitatively consistent with our experimental findings for CoPc(py)/CP. In contrast, CoPc/CP show no evidence of change in the Co oxidation state upon either reduction or oxidation under N₂, and a small change on oxidation under CO₂, suggesting that the redox events are primarily ligand-based for this 4-coordinate Co species. Previous studies conducted with structurally similar metal porphyrins have reported that axial ligation to the metal center modifies the electronic structure of the metal porphyrin and can alter whether redox events are porphyrin-based or metal-based.^{51, 52} We hypothesize that the difference in the redox mechanisms for

the surface immobilized CoPc/CP and CoPc(py)/CP is due to the fact that the axial pyridine ligand interacts with the Co orbitals to introduce more Co-character into the HOMO orbital, and this increased Co-mixing in the HOMO leads to an increased extent of Co-character in the redox events for the CoPc(py)/CP system. This hypothesized increase in the extent of Co-character in the HOMO orbital upon axial-coordination is supported by DFT studies of Co complexes with axial ligands CO (π -accepting) and HCN (σ -donating).^{28, 53}

In the case of CoPc-P4VP/CP under N₂, the energy and shape of the XANES edge shows similar qualitative shifts upon oxidation and reduction as those observed for CoPc(py)/CP, but the magnitude of these shifts is smaller (Figure 5e). Specifically, starting at the neutral complex at 0 V vs SCE, as we apply a more positive potential of 1.2 V vs SCE, there is an edge shift to slightly higher energy and when we apply a more negative potential of -0.5 V vs SCE, there is an edge shift to lower energy. There is no additional change in edge position when applying an even more negative potential of -1.25 V vs SCE. The magnitude of the edge shifts at 1.2 V vs SCE and -0.5 V vs SCE under N₂ are detectable but smaller in magnitude than those observed for CoPc(py)/CP, suggesting that the oxidation and the first reduction in CoPc-P4VP/CP have some Co-character but are not exclusively metal-centered. The decreased magnitude of the edge-shift in CoPc-P4VP/CP compared to CoPc(py)/CP could be due to the pyridyl groups in P4VP having less ability to donate electron density to the Co center in CoPc-P4VP compared to the free pyridine ligands in CoPc(py). This hypothesis is supported by the lower pK_a of pyridyl groups in P4VP compared to free pyridine.⁵⁴ The less electron-donating pyridyls in the polymer may result in weaker axial ligation of the pyridyl groups to the Co center in CoPc-P4VP/CP, leading to decreased Co-mixing in the HOMO and thus less extent of Co-character in the redox events for CoPc-P4VP/CP compared to CoPc(py)/CP. Under CO₂, CoPc-P4VP/CP still shows an edge-shift upon oxidation similar to that observed under N₂. However, under CO₂, there is no change in edge energy upon reduction even at the most negative applied potentials (Figure 5f).

The Role of Co Center in CoPc for CO₂RR

Our *in situ* electrochemical XANES experimental results suggest that reductions of the parent 4-coordinate CoPc do not involve Co-based oxidation state changes, whereas the 5-coordinate CoPc(py) does change oxidation state upon the first reduction event, which is not consistent with the previously reported mechanistic hypothesis and DFT computation results for CoPc.^{10, 11, 26-32} In the case of CoPc, the lack of redox activity at the Co center might suggest that the Co could be replaced with a redox-inactive metal, or even completely removed from the Pc ligand,

and the system might still retain activity for CO₂RR. Although we find this argument somewhat unlikely, to test if Co center is necessary for CO₂RR we measured the electrocatalytic CO₂RR activities and product distributions of ZnPc and the metal-free H₂Pc immobilized onto EPG electrodes and compared them to those measured for CoPc/EPG in previously reported studies.¹⁹ The results are summarized in Figure 6.

From our CPE studies, we found that the metal-free H₂Pc/EPG exposed to pH 5 phosphate electrolyte under 1 atm CO₂ exhibits negligible CO₂RR activity and mostly HER activity as has been previously reported,⁵⁵ which suggests that a metal site is needed to help coordinate and reduce CO₂. For comparison, ZnPc/EPG under similar conditions does show some activity for the CO₂RR, but operates with a turnover frequency for CO production (TOF_{CO}) $\sim 3 \times$ lower than that of CoPc/EPG and a lower Faradaic efficiency (ϵ) for CO production. These results suggest that the Co center plays an important role in CO₂RR in CoPc even though the redox activity appears to be mainly ligand based according to the *in situ* XANES data. To further probe the role of metal center, additional CVs for ZnPc and CoPc complexes dissolved in homogenous DMSO solutions were measured as shown in Figure S11. The shifts of redox couples of CoPc compared to ZnPc demonstrate that the Co center in CoPc influences the energy of molecular orbitals of the metal phthalocyanine complex even if the Co center itself does not show a change in oxidation state upon oxidation or reduction.

Note that when ZnPc is immobilized in P4VP, the resulting adsorbed ZnPc-P4VP/EPG has similar TOF_{CO} compared to that of ZnPc/EPG, but with lower overall activity due to inhibition of competitive HER and enhancing the CO₂ concentration within the polymer²⁶ as evidenced by the higher Faradaic efficiency for CO production. When compared to CoPc-P4VP/EPG, the TOF_{CO} of ZnPc-P4VP/EPG is $\sim 25 \times$ lower. These results suggests that pyridyl groups in P4VP either do not axially coordinate with ZnPc in ZnPc-P4VP/EPG, or any axial coordination does not result in enhanced catalytic activity.

The fact that the ZnPc/EPG has only $3 \times$ less activity than CoPc/EPG, as compared to the $\sim 25 \times$ lower activity for ZnPc-P4VP/EPG compared to CoPc-P4VP/EPG, is consistent with our proposal that the redox-activity in the 4-coordinate CoPc systems are primarily ligand based (Scheme 2.i), whereas the redox-activity in the 5-coordinate CoPc-P4VP systems has more metal-character (Scheme 2.ii). Because Zn is not expected to show metal-based redox activity under these conditions, the fact that ZnPc/EPG shows activity in the same order of magnitude as CoPc-EPG is consistent with the metal center in both cases being necessary for CO₂ coordination/reduction, but

not necessarily the site of primary redox activity. For comparison, the fact that CoPc-P4VP/EPG has dramatically-enhanced ($\sim 25 \times$ higher) activity compared to Zn-P4VP/EPG is consistent with our assertion that the two metal centers have dramatically-different roles in these two systems. One explanation for such a dramatic difference is that the axial-coordination of the pyridyl groups to the Co center in the CoPc-P4VP/EPG system results in a 5-coordinate Co center with a greater degree of redox activity, whereas the redox-activity is still likely ligand-based in the ZnPc-P4VP/EPG system regardless of whether the Zn is axially-coordinated to a pyridyl group. Thus, these activity results are qualitatively consistent with the assertions regarding the center of redox activity from our XANES experiments.

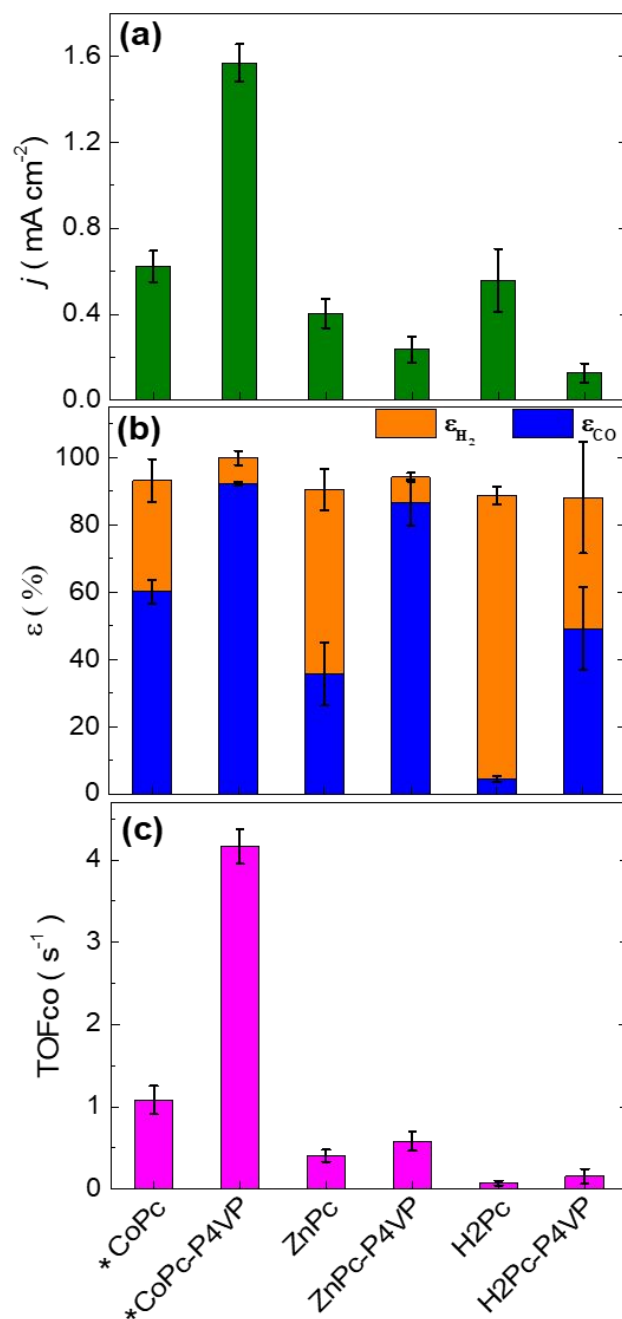


Figure 6. CPE results for CoPc, ZnPc, H₂Pc and related systems all adsorbed onto EPG electrodes. (a) overall current density; (b) Faradaic efficiencies for H₂ (orange bar) and CO (blue bar); and (c) turnover frequency for CO production. All measurements conducted in pH 5 phosphate solutions under CO₂ atmosphere at -1.25 V vs. SCE. All reported values are averages from 3 or more independent measurements, and the errors are given as standard deviations. *CoPc and *CoPc-P4VP data are from reference 19.

Conclusions

In this work, we used *in situ* electrochemical XAS to study the oxidation state and coordination environment of Co as a function of applied potential for CoPc, CoPc-P4VP, and CoPc(py) adsorbed onto carbon paper electrodes. We show that the coordination environment of Co changes from 4-coordinate in CoPc/CP to 5-coordinate in CoPc(py)/CP, and that CoPc-P4VP/CP exists mostly, although perhaps not completely, as a 5-coordinate Co complex. The Co coordination environment is not influenced by solution pH or applied potential for all three samples. However, the apparent Co oxidation state, as judged by the edge energy, is largely independent of applied potential for 4-coordinate CoPc but shows a potential-dependent shift for 5-coordinate CoPc-P4VP and CoPc(py), suggesting that the primary-coordination sphere effects have an important role in modulating the steady-state oxidation state of Co under catalytic turnover conditions. These findings corroborate our previous hypotheses regarding coordination environment of CoPc and related systems under applied potential and provide new important mechanistic insights regarding the electronic structure of CoPc under CO₂RR conditions.

Conflicts of interest

There are no conflicts to declare.

Acknowledgements

We thank Molly MacInnes and Robert Bonsall for their assistance with the collection of XANES measurements. We also acknowledge useful discussions with Nicolai Lehnert. This work was supported by an NSF-CAREER grant (CHE-1751791). Y. L. was partially supported by a Rackham One-Term Dissertation Fellowship by the University of Michigan. W.-X. N. was partially supported by a Margaret & Herman Sokol Graduate Summer Research Fellowship by the University of Michigan. W.S.D. acknowledges support by the National Science Foundation Graduate Research Fellowship Program (DGE-1256260). C. C. L. M. is a Cottrell Scholar of the Research

Corporation for Science Advancement. The authors acknowledge Stanford Synchrotron Radiation Lightsource for providing the beam time to perform the *in situ* XAS measurements.

References

1. E. E. Benson, C. P. Kubiak, A. J. Sathrum and J. M. Smieja, *Chem. Soc. Rev.*, 2009, **38**, 89-99.
2. J. L. Inglis, B. J. MacLean, M. T. Pryce and J. G. Vos, *Coord. Chem. Rev.*, 2012, **256**, 2571-2600.
3. A. M. Appel, J. E. Bercaw, A. B. Bocarsly, H. Dobbek, D. L. DuBois, M. Dupuis, J. G. Ferry, E. Fujita, R. Hille, P. J. A. Kenis, C. A. Kerfeld, R. H. Morris, C. H. F. Peden, A. R. Portis, S. W. Ragsdale, T. B. Rauchfuss, J. N. H. Reek, L. C. Seefeldt, R. K. Thauer and G. L. Waldrop, *Chem. Rev.*, 2013, **113**, 6621-6658.
4. J. Qiao, Y. Liu, F. Hong and J. Zhang, *Chem. Soc. Rev.*, 2014, **43**, 631-675.
5. A. J. Martín, G. O. Larrazábal and J. Pérez-Ramírez, *Green Chemistry*, 2015, **17**, 5114-5130.
6. T. P. Senftle and E. A. Carter, *Acc. Chem. Res.*, 2017, **50**, 472-475.
7. D. T. Whipple and P. J. A. Kenis, *The Journal of Physical Chemistry Letters*, 2010, **1**, 3451-3458.
8. P. De Luna, C. Hahn, D. Higgins, S. A. Jaffer, T. F. Jaramillo and E. H. Sargent, *Science*, 2019, **364**, eaav3506.
9. W. W. Kramer and C. C. L. McCrory, *Chem. Sci.*, 2016, **7**, 2506-2515.
10. N. Han, Y. Wang, L. Ma, J. Wen, J. Li, H. Zheng, K. Nie, X. Wang, F. Zhao, Y. Li, J. Fan, J. Zhong, T. Wu, D. J. Miller, J. Lu, S.-T. Lee and Y. Li, *Chem*, 2017, **3**, 652-664.
11. M. Zhu, R. Ye, K. Jin, N. Lazouski and K. Manthiram, *ACS Energy Lett.*, 2018, **3**, 1381-1386.
12. H. Wu, M. Zeng, X. Zhu, C. Tian, B. Mei, Y. Song, X.-L. Du, Z. Jiang, L. He, C. Xia and S. Dai, *ChemElectroChem*, 2018, **5**, 2717-2721.
13. Y. Cheng, J.-P. Veder, L. Thomsen, S. Zhao, M. Saunders, R. Demichelis, C. Liu, R. De Marco and S. P. Jiang, *J. Mater. Chem. A*, 2018, **6**, 1370-1375.
14. E. Boutin, M. Wang, J. C. Lin, M. Mesnage, D. Mendoza, B. Lassalle-Kaiser, C. Hahn, T. F. Jaramillo and M. Robert, *Angew. Chem. Int. Ed.*, 2019, **58**, 16172-16176.
15. Y. Wu, Z. Jiang, X. Lu, Y. Liang and H. Wang, *Nature*, 2019, **575**, 639-642.
16. J. Choi, P. Wagner, S. Gambhir, R. Jalili, D. R. MacFarlane, G. G. Wallace and D. L. Officer, *ACS Energy Lett.*, 2019, **4**, 666-672.
17. M. Wang, K. Torbensen, D. Salvatore, S. Ren, D. Joulié, F. Dumoulin, D. Mendoza, B. Lassalle-Kaiser, U. Işci, C. P. Berlinguette and M. Robert, *Nat. Commun.*, 2019, **10**, 3602.
18. M. Zhu, J. Chen, R. Guo, J. Xu, X. Fang and Y.-F. Han, *Applied Catalysis B: Environmental*, 2019, **251**, 112-118.

19. Y. Liu and C. C. L. McCrory, *Nat. Commun.*, 2019, **10**, 1683.
20. J. S. Zeng, N. Corbin, K. Williams and K. Manthiram, *ACS Catal.*, 2020, **10**, 4326-4336.
21. A. De Riccardis, M. Lee, R. V. Kazantsev, A. J. Garza, G. Zeng, D. M. Larson, E. L. Clark, P. Lobaccaro, P. W. W. Burroughs, E. Bloise, J. W. Ager, A. T. Bell, M. Head-Gordon, G. Mele and F. M. Toma, *ACS Applied Materials & Interfaces*, 2020, **12**, 5251-5258.
22. Z. Yang, X. Zhang, C. Long, S. Yan, Y. Shi, J. Han, J. Zhang, P. An, L. Chang and Z. Tang, *CrystEngComm*, 2020, **22**, 1619-1624.
23. X. Zhang, Z. Wu, X. Zhang, L. Li, Y. Li, H. Xu, X. Li, X. Yu, Z. Zhang, Y. Liang and H. Wang, *Nat. Commun.*, 2017, **8**, 14675.
24. J. Wang, X. Huang, S. Xi, J.-M. Lee, C. Wang, Y. Du and X. Wang, *Angew. Chem. Int. Ed.*, 2019, **58**, 13532-13539.
25. C. M. Lieber and N. S. Lewis, *J. Am. Chem. Soc.*, 1984, **106**, 5033-5034.
26. T. Yoshida, K. Kamato, M. Tsukamoto, T. Iida, D. Schlettwein, D. Wöhrle and M. Kaneko, *J. Electroanal. Chem.*, 1995, **385**, 209-225.
27. T. Abe, T. Yoshida, S. Tokita, F. Taguchi, H. Imai and M. Kaneko, *J. Electroanal. Chem.*, 1996, **412**, 125-132.
28. M.-S. Liao and S. Scheiner, *J. Chem. Phys.*, 2001, **114**, 9780-9791.
29. B. R. Kozub and R. G. Compton, *Sensors and Actuators B: Chemical*, 2010, **147**, 350-358.
30. F. Bedioui, E. De Boysson, J. Devynck and K. J. Balkus, *J. Electroanal. Chem. Interfacial Electrochem.*, 1991, **315**, 313-318.
31. H. A. Dinçer, A. Koca, A. Gül and M. B. Koçak, *Dyes and Pigments*, 2008, **76**, 825-831.
32. D. Kulaç, M. Bulut, A. Altındal, A. R. Özkaya, B. Salih and Ö. Bekaroğlu, *Polyhedron*, 2007, **26**, 5432-5440.
33. W. I. Dzik, J. I. van der Vlugt, J. N. H. Reek and B. de Bruin, *Angew. Chem. Int. Ed.*, 2011, **50**, 3356-3358.
34. A. L. Smith, K. I. Hardcastle and J. D. Soper, *J. Am. Chem. Soc.*, 2010, **132**, 14358-14360.
35. A. L. Smith, L. A. Clapp, K. I. Hardcastle and J. D. Soper, *Polyhedron*, 2010, **29**, 164-169.
36. J. Janczak and R. Kubiak, *Inorg. Chim. Acta*, 2003, **342**, 64-76.
37. F. Cariati, D. Galizzioli, F. Morazzoni and C. Busetto, *J. Chem. Soc., Dalton Trans.*, 1975, DOI: 10.1039/DT9750000556, 556-561.
38. W. McMaster, N. Del Grande, J. Mallett and J. Hubbell, *Compilation of x-ray cross-sections*, Lawrence Livermore National Laboratory: Livermore, CA, 1969.
39. T.-C. Weng, G. S. Waldo and J. E. Penner-Hahn, *Journal of Synchrotron Radiation*, 2005, **12**, 506-510.
40. A. R. Harutyunyan, A. A. Kuznetsov, O. A. Kuznetsov and O. L. Kaliya, *J. Magn. Magn. Mater.*, 1999, **194**, 16-21.

41. W. Shi-Kang, Z. Hou-Chen, C. Guo-Zhu, X. Da-Nian and X. Hui-Jun, *Acta Chimica Sinica English Edition*, 1985, **3**, 21-25.
42. E. Liaudet, F. Battaglini and E. J. Calvo, *J. Electroanal. Chem. Interfacial Electrochem.*, 1990, **293**, 55-68.
43. Y. Liu, K. Y. Leung, S. E. Michaud, T. L. Soucy and C. C. L. McCrory, *Comments Inorg. Chem.*, 2019, **39**, 242-269.
44. J. P. Krogman, J. R. Gallagher, G. Zhang, A. S. Hock, J. T. Miller and C. M. Thomas, *Dalton Trans.*, 2014, **43**, 13852-13857.
45. B. Hu, A. "Bean" Getsoian, N. M. Schweitzer, U. Das, H. Kim, J. Niklas, O. Poluektov, L. A. Curtiss, P. C. Stair, J. T. Miller and A. S. Hock, *J. Catal.*, 2015, **322**, 24-37.
46. L. S. Kau, D. J. Spira-Solomon, J. E. Penner-Hahn, K. O. Hodgson and E. I. Solomon, *J. Am. Chem. Soc.*, 1987, **109**, 6433-6442.
47. S. E. Shadle, J. E. Penner-Hahn, H. J. Schugar, B. Hedman, K. O. Hodgson and E. I. Solomon, *J. Am. Chem. Soc.*, 1993, **115**, 767-776.
48. J.-P. Dodelet, in *N4-Macrocyclic Metal Complexes*, eds. J. H. Zagal, F. Bedioui and J.-P. Dodelet, Springer New York, New York, NY, 2006, DOI: 10.1007/978-0-387-28430-9_3, pp. 83-147.
49. N. C. Tomson, K. D. Williams, X. Dai, S. Sproules, S. DeBeer, T. H. Warren and K. Wieghardt, *Chem. Sci.*, 2015, **6**, 2474-2487.
50. H. C. Brown and X. R. Mihm, *J. Am. Chem. Soc.*, 1955, **77**, 1723-1726.
51. P. Cocolios and K. M. Kadish, *Isr. J. Chem.*, 1985, **25**, 138-147.
52. A. B. P. Lever and J. P. Wilshire, *Can. J. Chem.*, 1976, **54**, 2514-2516.
53. M.-S. Liao and S. Scheiner, *J. Chem. Phys.*, 2002, **117**, 205-219.
54. Y. E. Kirsh and O. P. Komarova, *Polymer Science U.S.S.R.*, 1976, **18**, 223-228.
55. N. Furuya and K. Matsui, *J. Electroanal. Chem. Interfacial Electrochem.*, 1989, **271**, 181-191.

TOC Figure

